INTERNATIONAL JOURNAL FOR NUMERICAL METHODS IN FLUIDS, VOL. 10, 791–809 (1990)

DYNAMIC SIMULATION OF THE HYDRODYNAMIC INTERACTION AMONG IMMERSED PARTICLES IN STOKES FLOW

MARC S. INGBER

Department of Mechanical Engineering, University of New Mexico, Albuquerque, NM 87131, U.S.A.

SUMMARY

A numerical method for the dynamic simulation of the hydrodynamic interaction among particles in Stokes flow is developed. The method couples the quasi-static Stokes equations for the fluid with the equilibrium equations for the particles. The boundary element method is used to represent the velocity at a general field point in terms of surface velocities and stresses. However, neither the stresses nor the velocities are assumed to be known on the surface of the particles. Kinematic equations relating the linear and angular velocities at the centroids of the particles to the surface velocities are combined with the discretized boundary element equations and the equilibrium equations to generate a system of linear equations. The associated coefficient matrix is correspondent to the grand resistance matrix which relates the velocities of the particles to a given geometry.

KEY WORDS Stokes flow Hydrodynamic interactions Suspension flows Two-phase flows Boundary element method

INTRODUCTION

The hydrodynamic interaction among immersed particles plays an important role in several problems of interest to scientists and engineers, including constitutive equation modelling, falling ball rheometry, pipeline transport of slurries, petroleum recovery, composite materials processing, blood flow and many more. The solution of the many-body problem is an essential component in the development of a predictive capability for particle flows even at relatively dilute concentrations. Several theoretical investigations of dilute concentrations of suspensions have been performed including those of Einstein,[1] Batchelor,[2] Jeffrey and Acrivos,[3] Brenner,[4] Brenner and O'Neill[5] and Hinch.[6] In particular, Brenner and O'Neill[5] developed the concept of the grand resistance matrix multiparticle systems, which related the particle velocities to the hydrodynamic interaction forces at equilibrium. The extension of these theories to particles of complex shape has been limited because of the requirement of a detailed knowledge of the hydrodynamic interaction among the particles.

Several important advancements in the numerical simulation of the many-body problem have evolved over the past several years. Kynch,[7] Hocking[8] and Mazur and van Saarloos[9] used the method of reflections to determine the mobility functions (the inverse of the grand resistance matrix) for multiple-sphere systems. Gantos *et al.*,[10] using a boundary collocation method based on the expansion of the Stokes equations into appropriate eigenfunctions, studied the three-body problem. Most recently, Durlofsky *et al.*,[11] developed a method to calculate the resistance

0271–2091/90/070791–19$09.50
© 1990 by John Wiley & Sons, Ltd.
Received 14 April 1989

matrices for the multibody problem that accounted for the near-field lubrication effects. However, all of these methods are limited to systems of high symmetry to reduce the numbers of unknowns. Ingber[12] developed a method based on the boundary element method (BEM) which coupled the Stokes equations for the fluid with the rigid body equations of motion for the particles. Although the method was not limited to simple geometries and could be extended to the many-body problem, it was computationally expensive because of the stringent stability requirements demanded by the rigid body equations of motion. Tran-Cong and Phan-Thien[13] also developed a method based on the BEM to derive the grand resistance matrix. However, it was necessary for them to invert a fully populated matrix, making the use of this method expensive for dynamic simulation.

The present study is based on a quasi-steady analysis of multiple-particle Stokes flow interactions using the BEM. The present method differs from the author's previous work[12] in that the solution of the boundary element equations does not require knowledge of the velocity field. The velocity field is determined as part of the solution vector. In the quasi-steady analysis the rigid body equations of motion are circumvented and hence the accompanying stability problems are eliminated. Much larger time steps can be taken, making the present method computationally efficient. A wide variety of example problems are considered to show the advantages of the present method.

FORMULATION FOR MULTIPLE PARTICLES

We consider creeping flow in domain Ω with boundary Γ. The boundary Γ can be decomposed into the following components:

$$\Gamma = \Gamma_f + \sum_{i=1}^{N} \Gamma_i, \tag{1}$$

where Γ_f represents the fixed portion of the boundary (either real or imaginary) and Γ_i represents the surface of the ith particle. (For exterior flows Γ_f may not be present.) The governing differential equations in terms of the dimensionless perturbed fluid velocity u_i and the pressure p are given by

$$\frac{\partial^2 u_i(x)}{\partial x_j \partial x_j} = \frac{\partial p(x)}{\partial x_i}, \qquad \frac{\partial u_i(x)}{\partial x_i} = 0, \qquad x \in \Omega, \tag{2}$$

where Cartesian tensor notation is employed. Equation (2) can be recast in integral form by considering a weighted residual statement of the differential equations with weighting functions given by the fundamental solutions for the pressure and velocity.[12,14,15] The fundamental solution for the velocity field and the associated fundamental solution for the stress field are given by

$$u^*_{ij}(\xi, x) = \frac{1}{8\pi r}(\delta_{ij} + r_{,i} r_{,j}), \tag{3}$$

$$q^*_{ijk}(\xi, x) = \frac{-3}{4\pi} \frac{r_{,i} r_{,j} r_{,k}}{r^2}, \tag{4}$$

where r is the distance between ξ and x, δ_{ij} is the Dirac delta function and the comma denotes differentiation with respect to the appropriate Cartesian co-ordinate. The resulting boundary integral equation (BIE) is given by

$$c_{ij}(\xi) u_j(\xi) + \int_\Gamma q^*_{kji}(\xi, x) u_k(x) n_j(x) \mathrm{d}\Gamma = -\int_\Gamma u^*_{ik}(\xi, x) f_k(x) \mathrm{d}\Gamma, \tag{5}$$

where the f_k are the components of the traction along the surface Γ and the n_j are the components of the unit outward-normal vector to the boundary Γ. The coefficient tensor c_{ij} can be determined from the geometry or by integrating q^*_{kji} over Γ.[12]

The BIE is discretized by subdividing the boundary into boundary elements within which the velocity and stress components are given polynomial approximation with the use of Lagrangian shape functions. That is, within the eth element we approximate u_i and f_i as follows:

$$u_i(x)|_{\Gamma_e} \cong \sum_{j=1}^{n} u^e_{ij} N_j(x), \tag{6}$$

$$f_i(x)|_{\Gamma_e} \cong \sum_{j=1}^{n} f^e_{ij} N_j(x), \tag{7}$$

where u^e_{ij} and f^e_{ij} represent the values of the ith components of velocity and stress respectively at the jth node within the eth element and the $N_j(x)$ are the shape functions of the appropriate order. Using these approximations we write the discretized form of equation (5) as follows:

$$c_{ij}(\xi)u_j(\xi) + \sum_{e=1}^{\mathrm{NE}} \int_{\Gamma_e} q^*_{kji}(\xi, x) u^e_{kl} N_l(x) n_j(x) \mathrm{d}\Gamma = \sum_{e=1}^{\mathrm{NE}} \int_{\Gamma_e} u^*_{ik}(\xi, x) f^e_{kl} N_l(x) \mathrm{d}\Gamma, \tag{8}$$

where NE is the number of elements and repeated indices imply summation. By placing the field point ξ in equation (8) successively at the M nodes within the boundary elements, the following $3M$ linear algebraic equations are generated:

$$[H_{ij}]\{\tilde{u}_j\} = [G_{ij}]\{\tilde{f}_j\}, \tag{9}$$

where $\tilde{u}_j$ and $\tilde{f}_j$ represent the values of the components of velocity and stress respectively at the jth node.

In traditional boundary element methods in each co-ordinate direction either the stress component or velocity component is specified at the collocation nodes by the boundary conditions and equation (9) can be rearranged to solve for the remaining unknowns. In the present method the velocity components are specified along Γ_f, the fixed portion of the boundary. However, along the particle boundaries Γ_i neither the stresses nor the velocities are known. Under the assumption that the particles are rigid, the velocities on the surface of the particles can be related to the six components of linear and angular velocity at the centroids of the particles through a $3M \times 6N$ kinematic matrix $[K_{jl}]$. That is,

$$\{\tilde{u}_j\} = [K_{jl}]\{U_l\}, \tag{10}$$

where $\{U_l\}$ represents the velocities (linear and angular) at the centroids of the elements. The algebraic system is closed in the present quasi-static analysis by enforcing the equilibrium equations. That is, we demand that the resultant forces and moments on the particles generated by the surface stresses and any body forces equal zero. This neglect of the particle accelerations is consistent with the neglect of the acceleration within the fluid. The equilibrium equations for the ith particle are given by

$$\int_{\Gamma_i} \mathbf{n}\cdot\boldsymbol{\sigma} \mathrm{d}\Gamma + b^i = 0, \tag{11}$$

$$\int_{\Gamma_i} (q - q^i)(\mathbf{n}\cdot\boldsymbol{\sigma}) \mathrm{d}\Gamma = 0, \tag{12}$$

where $\boldsymbol{\sigma}$ is the total stress tensor, b^i is the body force acting on the ith particle and q^i is the

location of the centroid of the ith particle. These equations can be represented symbolically in matrix form in terms of the surface tractions as follows:

$$[M_{ij}]\{\tilde{f}_j\} = \{\tilde{b}_i\}, \tag{13}$$

where $[M_{ij}]$ is a $6N \times 3M$ matrix. Combining equations (9), (10) and (13) we obtain

$$\begin{bmatrix} [G_{ij}] & -[H_{ij}][K_{jl}] \\ [M_{ij}] & 0 \end{bmatrix} \begin{Bmatrix} \{\tilde{f}_j\} \\ \{U_l\} \end{Bmatrix} = \begin{Bmatrix} 0 \\ \{\tilde{b}_i\} \end{Bmatrix}. \tag{14}$$

This formulation is similar to the grand resistance matrix formulation in that the particle velocities are determined directly as a function of the geometry. However, it also contains information concerning the stress distribution on the surface of the particles. It has the advantage over previous grand resistance matrix formulations using the BEM in that no matrices are inverted in order to eliminate the stresses.

Once the particle velocities are determined using equation (14), the particles can be repositioned using a variety of integrators. In the example problems discussed in the next section a fifth-order variable-time-step Runge–Kutta method is used.

RESULTS

The boundary element portion of the numerical algorithm is benchmarked for both the exterior and interior problem. For the exterior problem we first consider the case of two identical spheres sedimenting side by side and compare the boundary element results with analytical results. We next consider horizontal chains of sedimenting spheres and compare the boundary element results with numerical results of Gantos *et al.*[10] For the interior problem the boundary element results are benchmarked by comparison with analytical results for a sphere in a cylinder under both the influence of gravity (no mean flow) and the influence of a mean Poiseuille flow (no gravity). Next several dynamic simulations are considered, including the sedimentation of systems of three spheres, a comparison of sedimenting spheroids and rods, the interaction of a sedimenting sphere with a neutrally buoyant spheroid or rod, and the movement of a spheroid through a contraction in Poiseuille flow.

Static benchmarks

The first set of static benchmark tests consists of two identical spheres sedimenting side by side. This problem is considered since the BEM results can be compared with the analytical results of Stimson and Jeffrey[16] and Goldman *et al.*[17] It is convenient to present the results in terms of dimensionless quantities. The characteristic length scale is given by the radius of the sphere, a, and the characteristic velocity is given in terms of the terminal sedimentation velocity U_t of an isolated sphere:[18]

$$U_t = 2a^2(\rho_s - \rho_f)g/9\mu, \tag{15}$$

where ρ_s is the density of the sedimenting particles, ρ_f is the density of the suspending fluid, g is the gravitational constant and μ is the dynamic viscosity. The drag correction factor λ and the non-dimensional angular velocity ω are then defined by

$$\lambda = U_t/U, \qquad \omega = a\tilde{\omega}/U_t, \tag{16}$$

where U is the sedimenting velocity of the spheres and $\tilde{\omega}$ is the dimensional angular velocity. In this static benchmark test we consider constant, linear and quadratic approximations for the

velocities and the stresses. In all cases the geometry is given quadratic approximation. The boundary element results and the associated absolute errors are shown for a centre-to-centre separation of 3·0862a in Table I and for a centre-to-centre separation of 2·2552a in Table II. The results are less accurate for the case where the centre-to-centre separation is smaller because not only are the stress gradients larger but also, since collocation points on one particle are closer to boundary elements on the other particle, the quadrature errors are larger owing to the singular nature of the fundamental solutions. Nevertheless, even when the gap distance between the two particles is approximately one-quarter of the radius, the boundary element method provides accurate results for all the discretizations shown in the tables. The discretizations using linear and quadratic elements yield slightly more accurate results than the constant elements. However, the improvement in the accuracy with the higher-order elements is not as large as might be expected considering previous boundary element studies using p-adaptive grid optimization.[19–21] There are two plausible explanations for the relatively small improvement. First, for all but the constant elements, collocation nodes are placed along the interelement boundaries where the C^0-Lagrangian elements used in this study have discontinuous slopes. At low Reynolds numbers the flow field is sensitive to small changes in geometry, and by placing collocation nodes along the interelement boundaries the effects of the discontinuous slopes are accentuated. Secondly, since the particles are in rigid body motion with moderate rotation rates, the velocity fields within the boundary elements have relatively small variation. Since the improvement in the solution was

Table I. BEM results for the drag correction factor and the non-dimensional angular velocity for the case of two identical spheres falling side by side with a centre-to-centre separation of 3·0862a. The analytical results are given by $\lambda = 0{\cdot}7945$ and $\omega = 0{\cdot}07750$

Degrees of freedom	Function interpolation	λ	Absolute error	ω	Absolute error
32	Constant	0·7924	0·0021	0·07845	0·00095
96	Constant	0·7934	0·0011	0·07817	0·00067
192	Constant	0·7942	0·0003	0·07810	0·00060
44	Linear	0·7926	0·0019	0·07848	0·00098
160	Linear	0·7942	0·0003	0·07808	0·00058
100	Quadratic	0·7937	0·0008	0·07814	0·00064
204	Quadratic	0·7944	0·0001	0·07785	0·00035

Table II. BEM results for the drag correction factor and the non-dimensional angular velocity for the case of two identical spheres falling side by side with a centre-to-centre separation of 2·2552a. The analytical results are given by $\lambda = 0{\cdot}7327$ and $\omega = 0{\cdot}1314$

Degrees of freedom	Function interpolation	λ	Absolute error	ω	Absolute error
32	Constant	0·7302	0·0025	0·1356	0·0042
96	Constant	0·7308	0·0019	0·1348	0·0034
192	Constant	0·7316	0·0009	0·1339	0·0025
44	Linear	0·7304	0·0023	0·1356	0·0042
160	Linear	0·7319	0·0008	0·1336	0·0022
100	Quadratic	0·7312	0·0015	0·1340	0·0026
204	Quadratic	0·7322	0·0005	0·1329	0·0015

only moderate when using the higher-order elements, constant elements were chosen for the dynamic simulations because of the economy they provided in terms of the CPU costs. An analysis of these CPU costs is provided with the next set of benchmark tests.

The next set of static benchmark tests consists of horizontal chains of up to 15 evenly spaced spheres sedimenting under the influence of gravity. The ratio of the centre-to-centre spacing to the

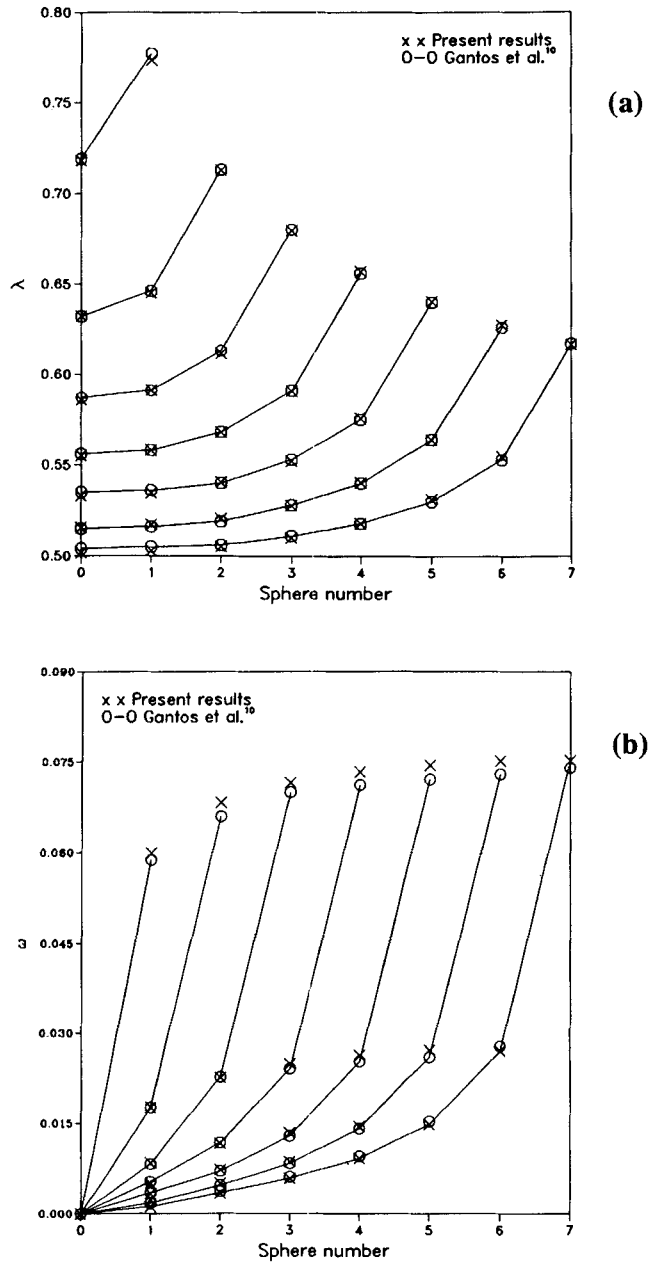

Figure 1. (a) Vertical drag reduction factors and (b) angular velocities for horizontal chains of spheres

sphere diameter is two. Comparisons between the present BEM results and the results of Gantos *et al.*[10] are shown in Figure 1 for the vertical drag correction factor λ and the non-dimensional angular velocity ω. Results for only half of the chain are shown because of the symmetry. The central sphere is designated by $j = 0$. The maximum discrepancy between the two sets of results is less than 0·2% for the drag reduction factor λ and less than 3·2% for the angular velocity ω. On the basis of the previous benchmark and similar convergence tests, each sphere was discretized into 16 superparametric elements in which the geometry was given quadratic approximation and the velocities and stresses were assumed to be constant within the elements. The CPU times ran from 3·7 CPU seconds for the three-sphere case up to 162 CPU seconds for the 15-sphere case on a Cray XMP timesharing system. A plot of the degrees of freedom (16 per sphere) versus the total CPU time is shown in Figure 2 for this example. It is seen that in the range from three to 15 spheres there is a quadratic scaling between degrees of freedom and the CPU cost. The major routines associated with the method are the numerical quadrature routine and the Gaussian elimination routine. Hence the operation count (OC) is estimated by

$$\mathrm{OC} = C_1 M^2 + C_2(M + 6N)^2 + C_3(M + 6N)^3, \tag{17}$$

where M is the number of degrees of freedom, N is the number of particles and C_1, C_2 and C_3 are constants. The first term on the right-hand side of equation (17) is associated with the quadrature routine and the second two terms are associated with the Gaussian elimination routine. In the light of the CPU times shown in Figure 2, we can conclude that C_1 must be much larger than C_3. This is substantiated by the fact that in all cases over 85% of the CPU time was spent in forming the linear system of equations. Presumably, for very large numbers of particles the cubic scaling would eventually predominate.

The next set of static benchmarks consists of a sphere inside a cylinder (Figure 3). The length of the cylinder is three times the diameter, although longer cylinders were considered without any

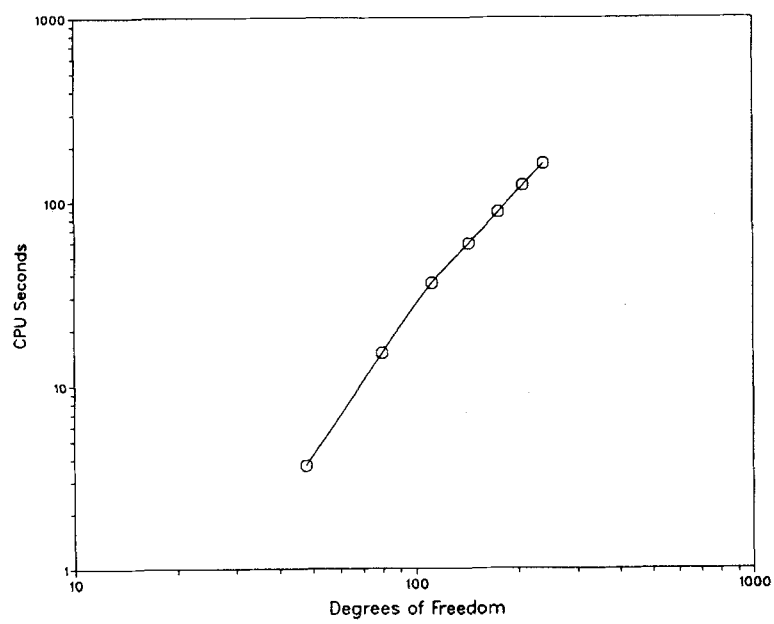

Figure 2. Relationship between degrees of freedom and the CPU cost for the case of the horizontal chains of spheres

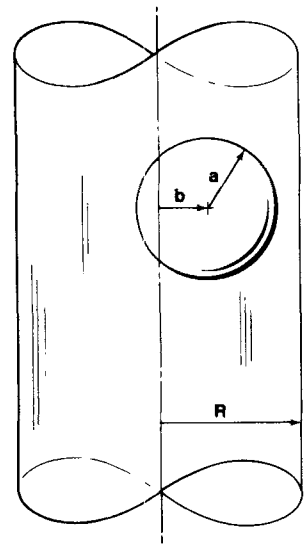

Figure 3. Problem geometry of a ball (diameter $2a$) sedimenting a distance b off the axis of a cylinder (diameter $2R$)

noticeable change in the results. First we consider spheres of varying diameter sedimenting along the centreline of the cylinder. We compare the wall correction factor K given by

$$K = \frac{\text{drag in the presence of the outer cylinder}}{\text{drag in an infinite medium}} \tag{18}$$

with the analytical results given by Happel and Brenner[18] in Figure 4. In all cases the sphere was discretized with 16 superparametric boundary elements and the cylinder was discretized with 186 superparametric boundary elements. As seen in Figure 4, errors increased with increasing sphere diameter, with a maximum error of 5·4% for $a/R = 0{\cdot}5$. Next we consider eccentric positioning of the sedimenting spheroid within the cylinder as characterized by the off-centre distance b for the ratio $a/R = 0{\cdot}135$. The ratio of the wall correction factor for $b/R = 0$ to the wall correction factor for $b/R \neq 0$ as a function of b/R is shown in Figure 5. The results are compared with a theoretical prediction proposed by Graham *et al.*[22] The present results match the theoretical predictions quite well. As the ball is moved off centre the sedimentation velocity is actually increased despite the fact that the ball is closer to the wall. The reason for this is that as the ball moves off centre the rotation rate is increased, which enhances the sedimentation rate. Eventually, as the eccentricity is increased the close proximity of the wall will cause the sedimentation velocity to decrease. The eccentric position at which the drag is minimized is approximately 0·4. This matches the analytical prediction for small balls.[22,23] Finally we consider the case of a neutrally buoyant sphere moving under the influence of a Poiseuille flow inside a cylinder. The relationship between the lateral position and the velocity of the centre of the sphere, U_0, normalized by the mean velocity V_m in the undisturbed Poiseuille flow for the ratio $a/R = 0{\cdot}13$, is compared with the analytical results of Bungay and Brenner[24] in Figure 6. Again the present static boundary element analysis matches the theory quite well.

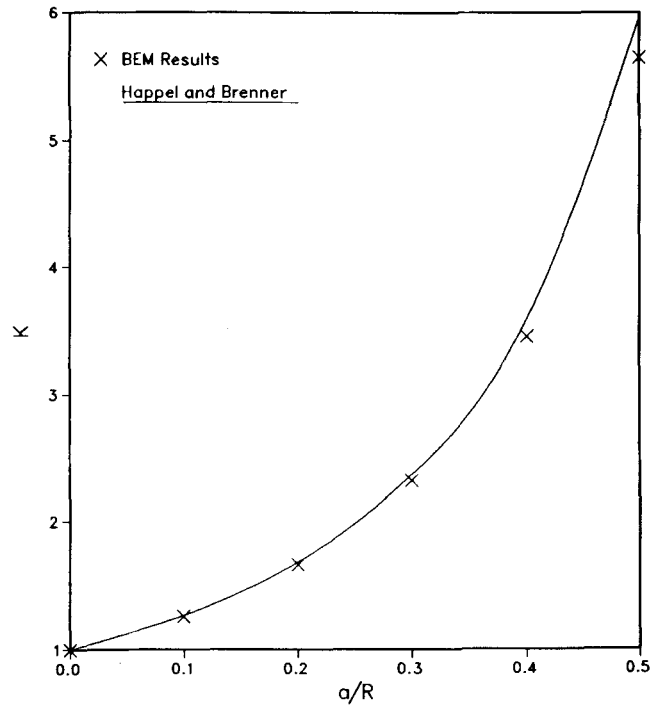

Figure 4. Wall correction factors for a sphere sedimenting along the axis of a cylinder

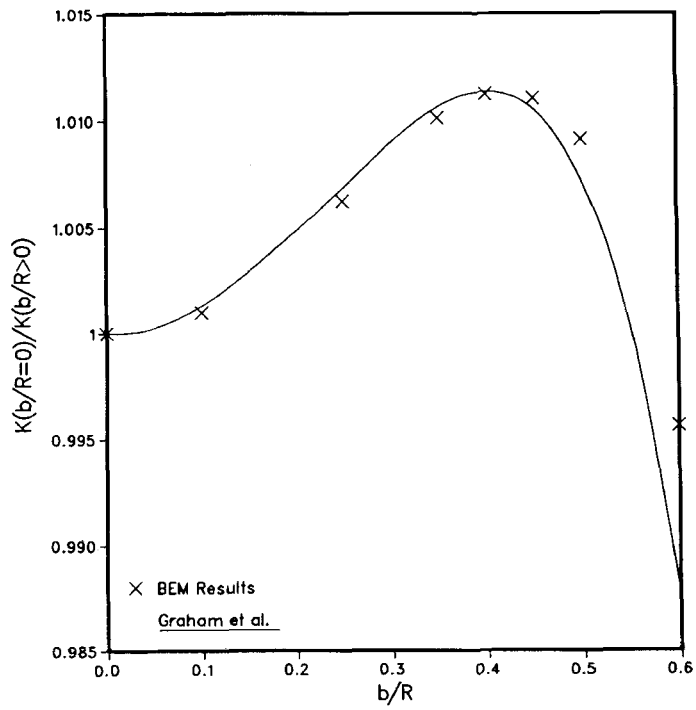

Figure 5. Ratio of the wall correction factor for the ball sedimenting along the axis of a cylinder ($b/R = 0$) to the wall correction factor for the ball sedimenting off centre ($b/R > 0$) for the case $a/R = 0{\cdot}135$

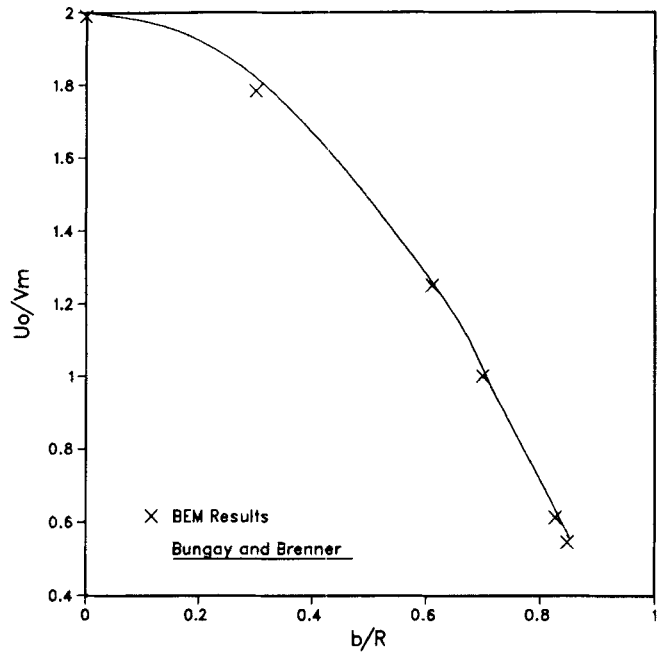

Figure 6. Velocity of a neutrally buoyant sphere under the influence of Poiseuille flow inside a cylinder for the case $a/R = 0{\cdot}13$

Dynamic simulations

We first consider sedimenting systems of three initially horizontal identical spheres. For each system the initial distance between the centres of the two outer spheres is six diameters and the relative position of the middle sphere is given in terms of the parameter $C = B/A$, where B is the centre-to-centre distance between the central sphere and the right outer sphere and A is the centre-to-centre distance between the central sphere and the left outer sphere. Configurations were run with values of C given by 1·1, 1·4, 1·5, 1·6 and 1·7. The trajectories for these systems are shown in Figure 7. This problem was investigated numerically by Gantos *et al.*[10] and Durlofsky *et al.*[11] and experimentally by Jayaweera *et al.*[25] Although Gantos *et al.* provided only snapshots which showed the relative orientations and rotations of the spheres, the present boundary element simulations match the results of Gantos *et al.* qualitatively. In certain cases, after the systems have sedimented for several diameters, two of the three spheres approach each other and essentially form a stable doublet. In these situations, because of the increase in the drag reduction factor,[12] the two spheres will separate from the third sphere. We number the spheres from left to right in their initial horizontal positions. As seen in Figure 7, sphere 1 is left behind for $C = 1{\cdot}1$ and $C = 1{\cdot}4$, sphere 3 is left behind for $C = 1{\cdot}5$ and sphere 2 is left behind for $C = 1{\cdot}6$ and $C = 1{\cdot}7$. These results have previously been observed numerically by Gantos *et al.* and experimentally by Jayaweera *et al.* Durlofsky *et al.* also considered the case for $C = 1{\cdot}4$. They used two variants of a simulation based on a reflection method, one which ignored the near-field lubrication effects and one which included the near-field lubrication effects. The trajectories of the two simulations were essentially the same through $z = -600$, at which point the trajectories diverged. Their more accurate method did not show sphere 1 lagging behind. The trajectory shown in Figure 7(b) is

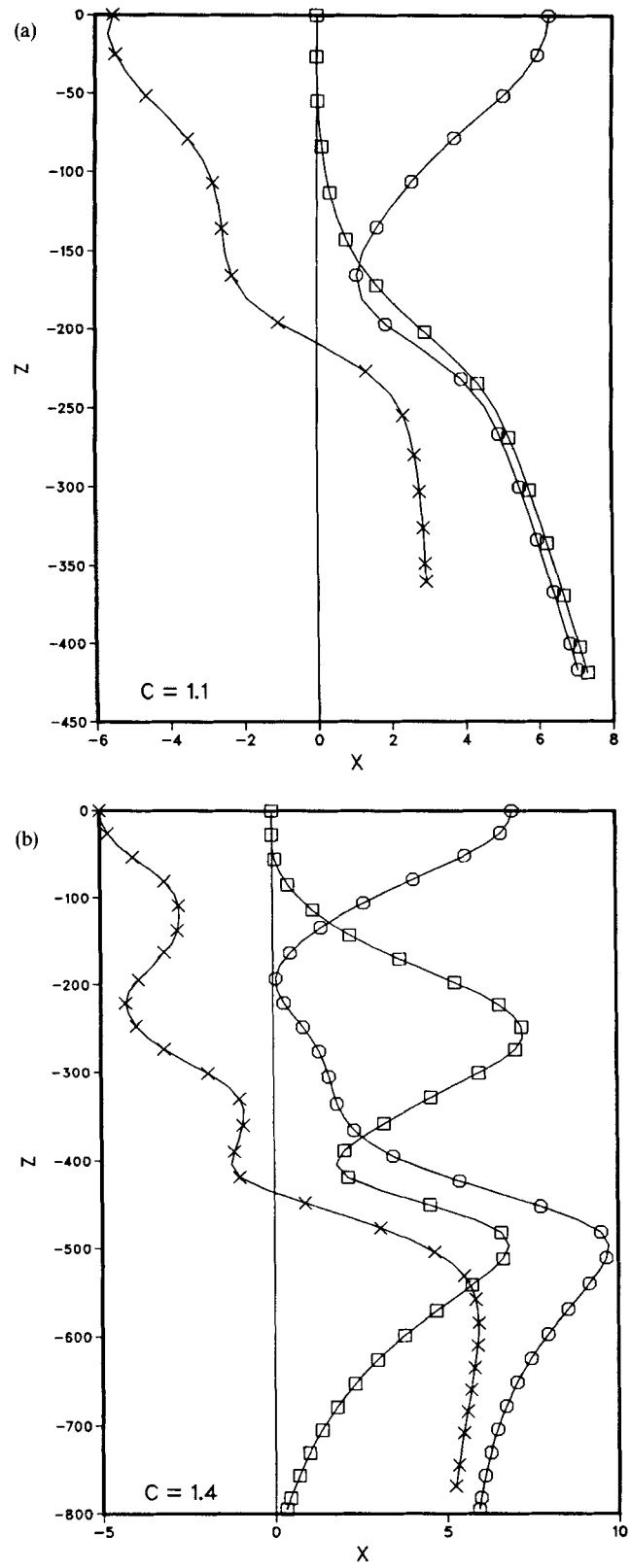
(a)
0
-50
-100
-150
-200
-250
-300
-350
-400
-450
Z
C = 1.1
-6
-4
-2
0
2
4
6
8
X
(b)
0
-100
-200
-300
-400
-500
-600
-700
-800
Z
C = 1.4
-5
0
5
10
X

Figure 7. (a, b)

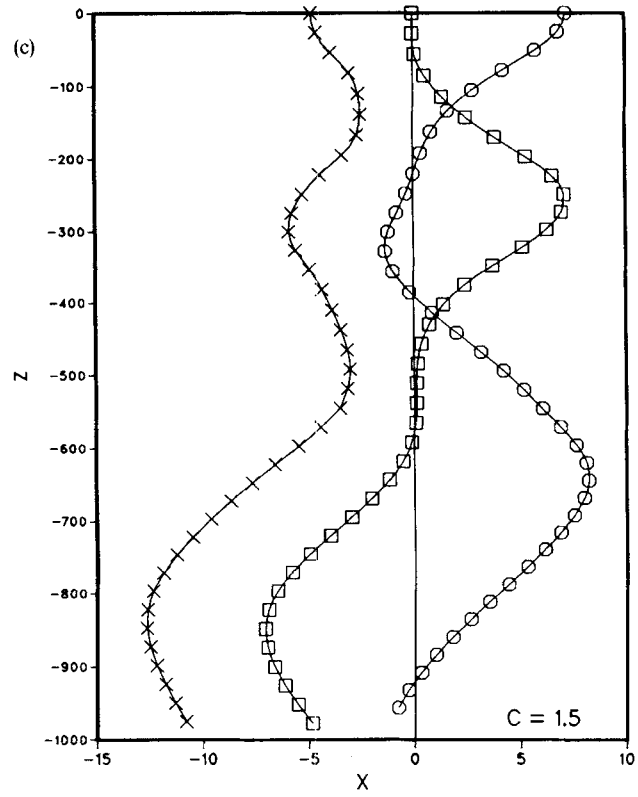
(c)
0
-100
-200
-300
-400
-500
-600
-700
-800
-900
-1000
Z
-15
-10
-5
0
5
10
X
C = 1.5

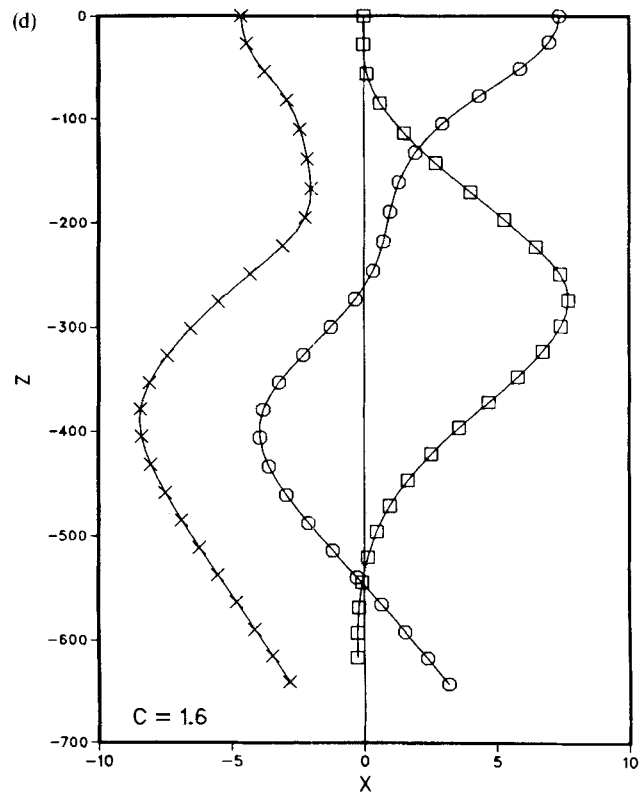
(d)
0
-100
-200
-300
-400
-500
-600
-700
Z
-10
-5
0
5
10
X
C = 1.6

Figure 7. (c, d)

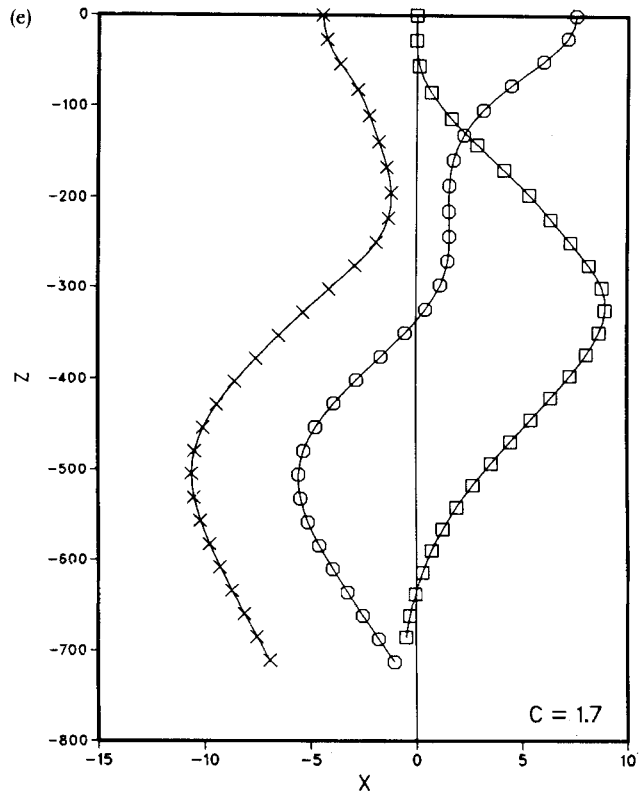

Figure 7. Chains of three unequally spaced spheres sedimenting under the influence of gravity. X and Z are measured in units of the sphere radius a and the increment between each plot symbol is 21·22 dimensionless time units where the characteristic time unit is given by a/U_t

essentially the same as that of Durlofsky *et al.* through sedimentation of 600 radii. As they mention in their paper, it is not surprising that the trajectories differ after some time because of the fact that the flow field is sensitive to small changes in geometry, especially for Stokes flow.

The next dynamic simulation considers the sedimentation of spheroids and rods. Spheroids have long been used to approximate rods[26] because of the simplification in the analysis that spheroids allow. We consider prolate spheroids and rods of aspect ratio 2 with an initial centre-to-centre spacing given by $R = 2{\cdot}5$ (Figure 8). The trajectories and orientations for the right particle of a pair of initially vertical spheroids as calculated by the present method are compared with the reflection results of Kim[27] in Figure 9. The two methods provide essentially the same results. These trajectories and orientations are compared with the trajectories and orientations for sedimenting rods. In the first case the rod of aspect ratio 2 is of the same length as the spheroid. It is seen in Figure 9(a) that the trajectory for the rod is quite different from that of the spheroid. The difference can be attributed in large part to the extra surface area of the rod compared to the spheroid. In the second case the rod is again given aspect ratio 2 but in this case the length of the rod is chosen so that the surface area is the same as that of the spheroid. The trajectory is closer to that of the spheroid than the longer rod but is still significantly different. In all cases the trajectories are periodic because of the symmetry in the Stokes equations. The particles rotate 90°

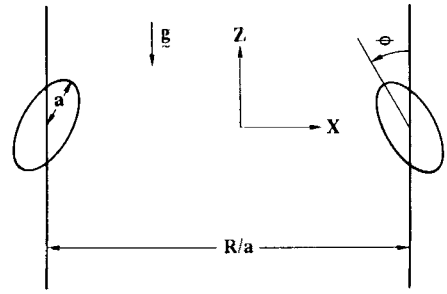

Figure 8. Problem geometry of two inclined spheroids (rods) sedimenting under the influence of gravity

in one half-period as they move apart and then follow a symmetric path during the next 90° of rotation as they move towards each other to complete the period. Normalizing the period for the spheroid to 1, the period of the long rod is 0·517 and the period of the shorter rod is 0·810. That is, the rotation rate of both rods is greater than that of the spheroid. The rotation rate is more sensitive to the shape differences between the rod and the spheroid than is the sedimenting velocity.

We next consider a system containing a sedimenting sphere and a neutrally buoyant spheroid or rod of aspect ratio 2 (Figure 10). This problem was first considered by Ingber[12] using a boundary element method coupled to the rigid body equations of motion. Because the present method does not possess the severe stability problems associated with the rigid body equations of motion, especially as the particles approach each other, the present method can utilize much larger time increments, thus making it far more efficient. Although the amount of savings depends on how close the particles come to each other during the simulation and the time-stepping algorithm, CPU savings in excess of 10 times were realized over the author's previous method. The positions of the centres of the particles for the system containing the sedimenting sphere and the neutrally buoyant spheroid are shown in Figure 11. The motion of the sedimenting sphere causes the neutrally buoyant particle to move vertically downwards and to rotate counter-clockwise. Initially, both particles move horizontally away from each other. After the centre of the sedimenting particle passes the vertical position of the centre of the spheroid, the two particles move horizontally towards each other as the spheroid is pulled into the wake of the sphere. The trajectories shown in Figure 11 are essentially the same as the author's previous results.[12] As in the dynamic simulation for the sedimenting spheroids and rods, a comparison was made to determine the effect of approximating a rod with a spheroid. Both a neutrally buoyant rod of aspect ratio 2 with the same length as the spheroid and a neutrally buoyant rod of aspect ratio 2 with the same surface area as the spheroid were again considered. These trajectories are not shown in Figure 10 because they are essentially the same as the spheroid trajectories shown in the figure. The maximum discrepancy in the vertical position, the horizontal position and the angular rotation between the spheroid and the longer rod was 0·7%, 0·07% and 3·5% respectively. The maximum discrepancy in the vertical position, the horizontal position and the angular rotation between the spheroid and the shorter rod was 0·5%, 0·07% and 2·5%, respectively. The difference in the trajectories is slightly smaller when comparing the rod with equivalent surface area to the spheroid. Nevertheless, unlike the previous simulation containing two sedimenting particles, very little error is introduced here by approximating a rod with a spheroid.

The final dynamic simulation considers a spheroid moving through a contraction under the influence of a Poiseuille flow. An abrupt contraction connects the upstream cylinder of diameter 8

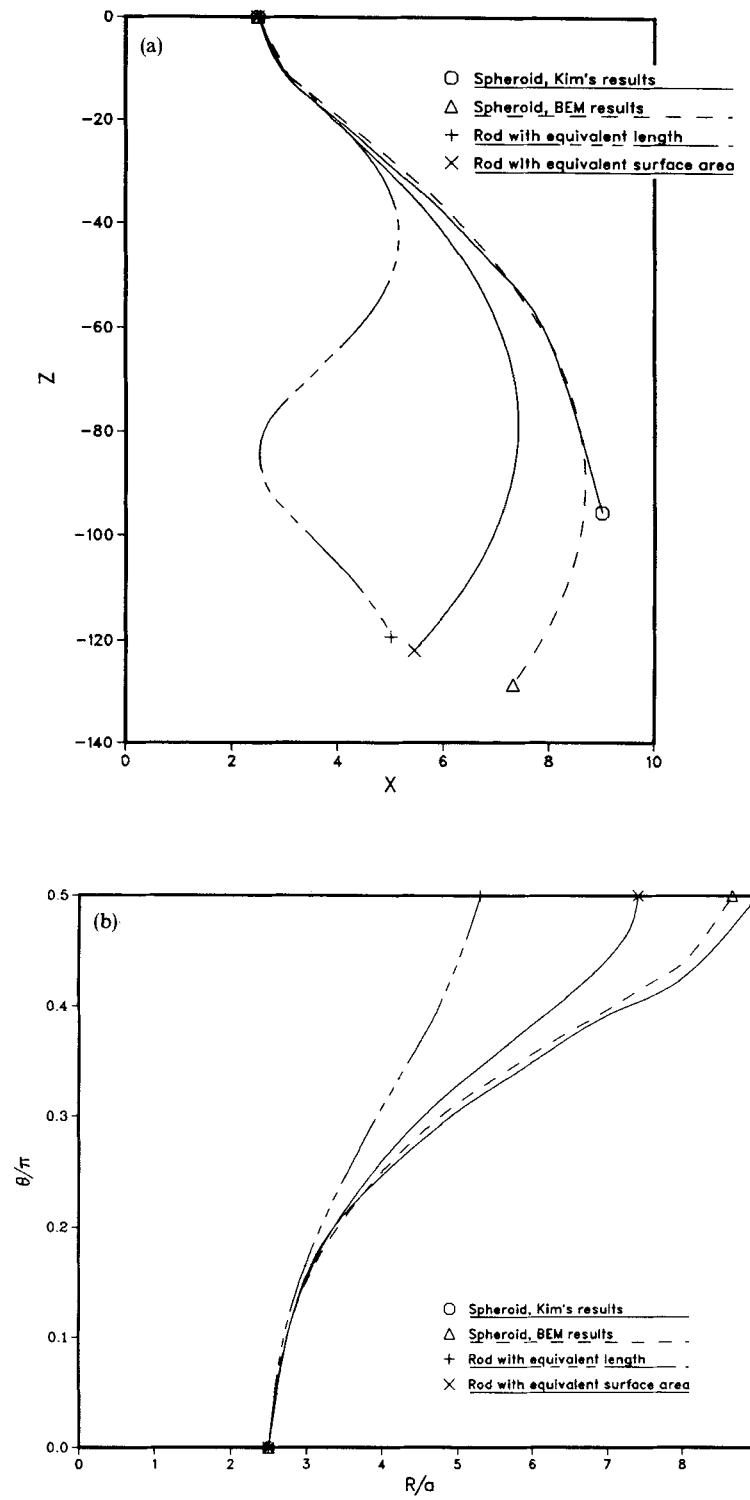

Figure 9. Comparison of (a) trajectories and (b) orientations for the systems containing two spheroids of aspect ratio 2, two rods of aspect ratio 2 with the same length as the spheroids, and two rods of aspect ratio 2 with the same surface area as the spheroids

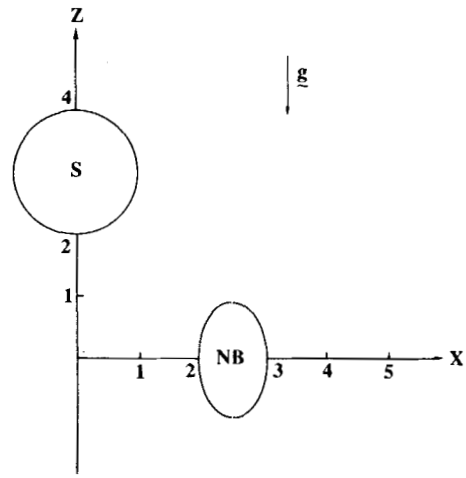

Figure 10. Problem geometry for a system composed of a sedimenting sphere (S) and a neutrally buoyant particle (NB)

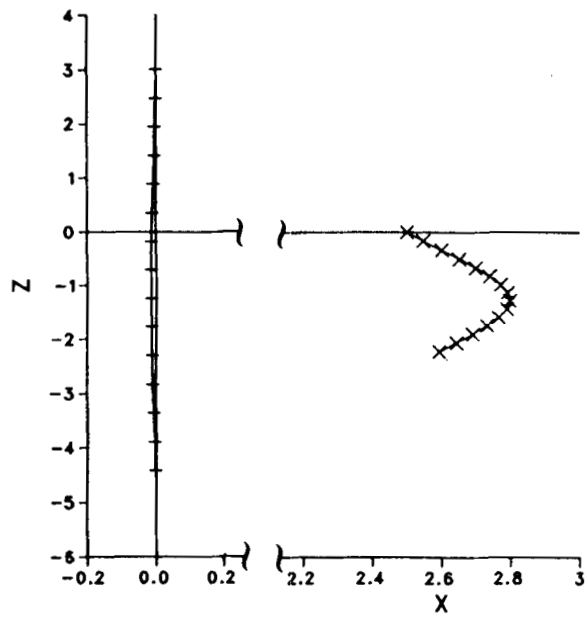

Figure 11. Trace of the locations of the centres of the sedimenting sphere (+) and the neutrally buoyant particle (×). The increment between each plot symbol is 0.265 dimensionless time units where the characteristic time unit is given by a/U_t

with the downstream cylinder of diameter 2. The upstream centreline velocity is 1. Prolate spheroids of aspect ratio 2 and length 1 are placed at three off-centre locations 6 units upstream of the contraction. The trajectories and orientations at 1 s intervals are shown in Figure 12. The spheroids rotate so that the major axis is almost horizontal as they move through the contraction. Once through the contraction, the spheroids undergo periodic rotational motion in a similar

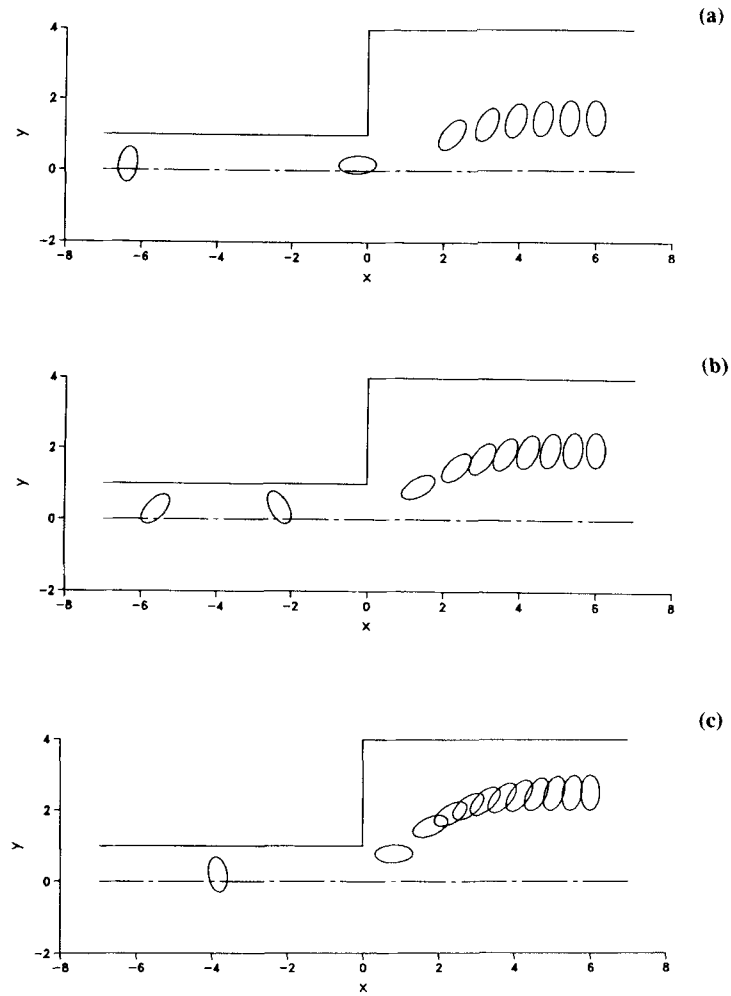

Figure 12. Spheroid moving through a contraction under the influence of a Poiseuille flow: (a) initial position $x=6$, $y=1{\cdot}5$; (b) initial position $x=6$, $y=2{\cdot}0$; (c) initial position $x=6$, $y=2{\cdot}5$. The increment between each plot symbol is 1·0 s

fashion to the Jeffery orbits of ellipses in Couette flow.[28] The length of time the spheroid takes to make it through the contraction increases with its initial distance off the centreline. As seen in Figure 11, the particle with centroid originally at $y = 1{\cdot}5$ took approximately 6 s to pass through the contraction, the particle with centroid originally at $y = 2{\cdot}0$ took between 7 and 8 s to pass through the contraction, and the particle with centroid originally at $y = 2{\cdot}5$ took over 10 s to pass through the contraction. Although there are no experiments with which to compare these results, they appear to be reasonable.

DISCUSSION

A numerical method which couples the Stokes equations for the fluid with the equilibrium equations for the particles has been developed for the dynamic simulation of the hydrodynamic

interaction among immersed particles in Stokes flow. The Stokes equations are solved using the boundary element method, which places no restrictions on the complexity of the geometry. The current formulation has two improvements over previous boundary element formulations. First, no matrices need be inverted in order to obtain an explicit expression for the surface tractions, and secondly, no stability problems have been encountered with the variable-time-step Runge–Kutta time integrator. These two improvements are key ones in making the present method viable for dynamic simulations. The method can be applied to both the exterior and interior problem (with or without mean flow) containing buoyant, neutrally buoyant and/or sedimenting particles.

In two of the example problems a comparison was made between spheroids and rod-like particles to determine the suitability of approximating rods with spheroids. In the case of the sedimenting particles there were significant differences between the trajectories of the spheroidal particles and the rod-like particles. These differences were mainly due to the variance in the rotation rates. However, in the case of the sedimenting sphere interacting with the neutrally buoyant rod or spheroid, the trajectories were essentially the same. This suggests that, to a large extent, the neutrally buoyant particle was simply moving with the flow field induced by the sedimenting sphere.

ACKNOWLEDGEMENTS

This work was supported by the National Science Foundation under grant MSM-8807914 and by Sandia National Laboratories and the U.S. Department of Energy under contract DE-AC04-76DP00789.

REFERENCES

1. A. Einstein, 'Eine neue Bestimmung der Moleküldimensionen', *Ann. Physik*, **19**, 289–306 (1906).
2. G. K. Batchelor, 'Sedimentation in a dilute dispersion of spheres', *J. Fluid Mech.*, **52**, 245–268 (1972).
3. D. J. Jeffrey and A. Acrivos, 'The rheological properties of suspensions of rigid particles', *AIChE J.*, **22**, 417–432 (1976).
4. H. Brenner, 'Rheology of a dilute suspension of axisymmetric Brownian particles', *Int. J. Multiphase Flow*, **1**, 195–341 (1974).
5. H. Brenner and M. E. O'Neill, 'On the Stokes resistance of multiparticle systems in a linear shear field', *Chem. Eng. Sci.*, **27**, 1421–1439 (1972).
6. E. J. Hinch, 'An averaged-equation approach to particle interaction in a fluid suspension', *J. Fluid Mech.*, **83**(4), 695–720 (1977).
7. G. J. Kynch, 'The slow motion of two or more spheres through a viscous fluid', *J. Fluid Mech.*, **5**, 193–208 (1959).
8. L. M. Hocking, 'The behavior of clusters of spheres falling in a viscous fluid. Part 2. Slow motion theory', *J Fluid Mech.*, **20**, 129–139 (1964).
9. P. Mazur and W. van Saarloos, 'Many-sphere hydrodynamic interactions and mobilities in a suspension', *Physica*, **115A**, 21–57 (1982).
10. P. Gantos, R. Pfeffer and S. Weinbaum, 'A numerical-solution technique for three-dimensional Stokes flows, with applications to the motion of strongly interacting spheres in a plane', *J. Fluid Mech.*, **84**(1), 79–111 (1978).
11. L. Durlofsky, J. F. Brady and G. Bossis, 'Dynamic simulation of hydrodynamically interacting particles', *J. Fluid Mech.*, **180**, 21–49 (1987).
12. M. S. Ingber, 'Numerical simulation of the hydrodynamic interaction between a sedimenting particle and a neutrally buoyant particle', *Int. j. numer. methods fluids*, **9**, 263–273 (1989).
13. T. Trans-Cong and N. Phan-Thien, 'Stokes problems of multiparticle systems: a numerical method for arbitrary flows', *Phys. Fluids A*, **1**(3), 453–461 (1989).
14. O. A. Ladyzhenskaya, *The Mathematical Theory of Viscous Incompressible Flow*, Gordon and Breach, New York, 1963.
15. G. K. Youngren and A. Acrivos, 'Stokes flow past a particle of arbitrary shape: a numerical method of solution', *J. Fluid Mech.*, **69**(2), 377–403 (1975).
16. M. Stimson and G. B. Jeffrey, 'The motion of two spheres in a viscous fluid', *Proc. R. Soc. A*, **111**, 110–116 (1926).
17. A. J. Goldman, R. G. Cox and H. Brenner, 'The slow motion of two identical arbitrarily oriented spheres through a viscous fluid', *Chem. Eng. Sci.*, **21**, 1151–1170 (1966).

18. J. Happel and H. Brenner, *Low Reynolds Number Hydrodynamics*, Martinus Nijhoff, Dordrecht, 1983.
19. A. Reverter, A. Gonzalez and E. Alarcon, 'Indicators and estimators in *p*-adaptive boundary elements', in C. A. Brebbia and G. Mair (eds), *Boundary Elements VII*, Springer-Verlag, Berlin, 1985.
20. E. Rank, 'Adaptive boundary element methods', in C. A. Brebbia, W. L. Wendland and G. Kuhn (eds), *Boundary Elements IX, Vol. 1*, Springer-Verlag, Berlin, 1987.
21. R. R. Chakravarty, 'Grid optimization for the boundary element method', *Master Thesis*, Iowa State University, 1988.
22. A. L. Graham, L. A. Mondy, J. D. Miller, N. J. Wagner and W. A. Cook, 'Numerical simulations of eccentricity and end effects in falling-ball rheometry', *J. Rheol.*, **33**(7), 1107–1128 (1989).
23. B. R. Hirschfeld, H. Brenner and A. Falade, 'First and second order wall effects upon the flow of viscous asymmetric motion of an arbitrarily-shaped, positioned, and oriented particle within a circular cylinder', *Phys. Chem. Hydrodyn.*, **5**(2), 99–133 (1984).
24. P. M. Bungay and H. Brenner, 'Pressure drop due to the motion of a sphere near the wall bounding a Poiseuille flow', *J. Fluid Mech.*, **60**(1), 81–96 (1973).
25. K. O. L. F. Jayaweera, B. J. Mason and G. W. Slack, 'The behavior of clusters of spheres falling in a viscous fluid. Part 1. Experiment', *J. Fluid Mech.*, **20**(1), 121–128 (1964).
26. R. G. Cox, 'The motion of long slender bodies in a viscous fluid. Part 1. General theory', *J. Fluid Mech.*, **44**(4), 791–810 (1970).
27. S. Kim, 'Sedimentation of two arbitrarily oriented spheroids in a viscous fluid', *Int. J. Multiphase Flow*, **11**(5), 699–712 (1985).
28. G. B. Jeffery, 'The motion of ellipsoidal particles immersed in a viscous fluid', *Proc. R. Soc. A*, **102**, 161–179 (1922).